Article

Crop Residue Burning Emissions and the Impact on Ambient Particulate Matters over South Korea

Kyung M. Han [1,2,*], Byung T. Lee [3], Min-Suk Bae [4], Sojin Lee [5], Chang H. Jung [6] and Hyun S. Kim [1]

[1] School of Earth Sciences and Environmental Engineering, Gwangju Institute of Science and Technology (GIST), Gwangju 61005, Korea; hskim98@gist.ac.kr
[2] Center for Earth Environmental Modeling Studies (CEMOS), Gwangju Institute of Science and Technology (GIST), Gwangju 61005, Korea
[3] Central Research Facilities, Gwangju Institute of Science and Technology (GIST), Gwangju 61005, Korea; btlee@gist.ac.kr
[4] Department of Environmental Engineering, Mokpo National University, Muan 58554, Korea; minsbae@mnu.ac.kr
[5] The Seoul Institute, Seoul 06756, Korea; slee@si.re.kr
[6] Department of Health Management, Kyung-in Women's University, Incheon 21041, Korea; jch@kiwu.ac.kr
* Correspondence: kman.han@gmail.com; Tel.: +82-62-715-3408

Abstract: In the study, crop residue burning (CRB) emissions were estimated based on field surveys and combustion experiments to assess the impact of the CRB on particulate matter over South Korea. The estimates of CRB emissions over South Korea are 9514, 8089, 4002, 2010, 172,407, 7675, 33, and 5053 Mg year^{-1} for PM_{10}, $PM_{2.5}$, OC, EC, CO, NO_x, SO_2, and NH_3, respectively. Compared with another study, our estimates in the magnitudes of CRB emissions were not significantly different. When the CRB emissions are additionally considered in the simulation, the monthly mean differences in $PM_{2.5}$ (i.e., $\triangle PM_{2.5}$) were marginal between 0.07 and 0.55 μg m^{-3} over South Korea. Those corresponded to 0.6–4.3% in relative differences. Additionally, the $\triangle PM_{10}$ was 0.07–0.60 μg m^{-3} over South Korea. In the spatial and temporal aspects, the increases in PM_{10} and $PM_{2.5}$ were high in Gyeongbuk (GB) and Gyeongnam (GN) provinces in June, October, November, and December.

Keywords: crop residue burning (CRB); emissions; $PM_{2.5}$; PM_{10}; WRF-CMAQ simulation; field survey; combustion experiment; South Korea

1. Introduction

The air quality in South Korea has been gradually improving over the past decades [1]. The recent concentrations of the particulate matter showed a rapid decline, in particular during the period of the coronavirus COVID-19 pandemic [2,3]. Nevertheless, there is still apprehension about serious air quality, and the annual average levels of PM_{10} and $PM_{2.5}$ do not meet the WHO air quality guidelines [4]. The South Korean government planned to reduce the $PM_{2.5}$ emissions by 35.8% by 2022 from 2014. To reduce the concentrations of particulate matter, the government has established policies (e.g., Special Act on Fine Aerosol) for each ministry and has implemented reduction measures as follows [3]:

- In energy production, conversion from coal-fired power plants to liquefied natural gas (LNG)-fired plants (i.e., coal-to-gas switching).
- In the industry section, extending the environmental management policy for total amount control of air pollutants from the Seoul Metropolitan area to the whole country.
- In transportation, early scrappage of old diesel vehicles and supply of low-emission vehicles such as electric and hybrid vehicles.

In the agricultural section, the South Korean government also strengthened the enforcement actions against illegal open burning activities. Nevertheless, as agricultural practices, crop residue burning (CRB) activities have been conducted in the field after

harvest to manage the large quantities of the crop residues and to provide some nutrients from the residues (e.g., ashes) into the soil [5,6]. However, there are few studies to quantify the CRB emission and examine their impacts on particulate matter in South Korea.

Similarly, the CRB has often occurred in China, India, Myanmar, Thailand, Laos, Cambodia, and Vietnam [7–11]. The emissions from crop residue burning (or biomass burning) activities are closely related to radiative effects, air pollution, and public health [12–15]. Crutzen and Andreae reported that gaseous species of CO, CH_4, NO_x, and VOCs from biomass burning influence the oxidation capacities of the atmosphere by reacting with OH radicals or elevating the levels of O_3 [13]. Particulate species emitted from the CRB can play a role in condensation nuclei leading to changes in radiative balance. In terms of air pollution, the peak concentrations of $PM_{2.5}$ due to the enhanced biomass burning emissions reached ~500 $\mu g\ m^{-3}$ in May 2012 in Chengdu, China [16]. Importantly, many investigators have attempted to estimate the biomass burning emissions based on bottom-up, top-down, and hybrid approaches on regional and global scales, particularly in China and India, as summarized in Table 1.

Generally, the emission fluxes are calculated by the multiplication of emission factors and dry masses of burned crop residues. In a conventional way (i.e., bottom-up (B) approach), the information on the dry mass of crop residues, agricultural waste burning, and its areas is obtained from statistical data and field surveys to farmers. The approach can lack accurate spatial and temporal allocations of the statistical and survey data. On the other hand, the remotely sensed observations (e.g., MODIS, SEVIRI, GOES) have been used to quantify the biomass burning emission [23,25,27,33,35,38,40,42,50–52]. The top-down emissions of biomass burning are estimated, multiplying several parameters of (i) burned areas, (ii) biomass load (FRP, fire radiative power), (iii) combustion efficiency (or conversion factor), and (iv) emission factors [53,54]. The typical products of the biomass burning (BB) emissions calculated from the MODIS sensor are the Fire Inventory from NCAR (FINN) and Global Fire Emissions Database (GFED) v3–v4, which are inventories, used worldwide to consider the BB emissions in the 3D-chemistry transport model simulations [36,55–57]. Figure 1 shows the spatial distributions of the annual carbon monoxide (CO) and black carbon (BC) emission fluxes from the FINNv1.5 inventory over East Asia for 2016. CO and BC are the main products of incomplete combustion of biomass burning.
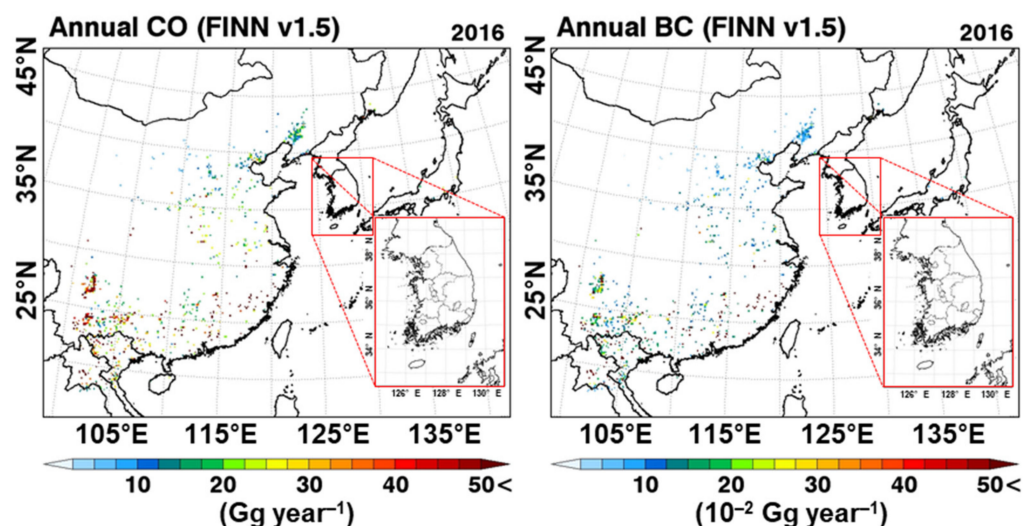
Figure 1. Annual emission fluxes of CO and BC from the FINNv1.5 inventory over East Asia. Their close-up of the area of South Korea.

Table 1. Several studies on the estimation of biomass burning emissions.

Refs	Estimation Method	Region	Periods	Parameters	Crops or land Types
Yang et al., 2008 [17]	B [a]	China (Suqian)	2001–2005	EF [b] (literatures), DM [c] (statistical data and field survey)	wheat, legume, rice, corn, potato, oil plant, cotton
Zhang et al., 2008 [18]	B	China	2004	EF (combustion chamber experiment), DM (field survey)	Rice, wheat, corn straws
Jain et al., 2014 [19]	B	India	2008–2009	EF (literature [20]), DM (field survey)	Rice paddy, wheat, maize, jute, cotton, groundnut, sugarcane, mustard, millets
Das et al., 2020 [11]	B	Nepal	2003–2017	EF (literature, [21,22]), DM (literatures)	Paddy, maize, millet, wheat, barley, oil crops, potatoes, sugarcane, jute, pluses
McCarty 2011 [23]	T [d]	USA	2003–2007	EF (literatures), DM (US EPA [24]), BA [e] (MODIS [f] sensor)	Bluegrass, corn, cotton, rice, soy, sugarcane, wheat, others
Liu et al., 2015 [25]	T	China (North Chain Plain)	2003–2014	EF (literatures [20,26]), conversion factor [27], BA with FRP [g] data (MODIS sensor)	wheat
Li et al., 2016 [28]	T	China	1990–2013	EF (literatures from experiments [29,30]), crop productions with grain-to-straw ratio (Chinese statistical data [31,32]), BA (MODIS sensor)	Wheat, corn, rice, cotton, others
Andela et al., 2016 [33]	T for burned crop residue	South America, Sub-Saharan Africa, and Australia	2003–2014	Conversion factor [27], BA with FRP data (MODIS and SEVIRI [h] sensors)	Cropland, woody savanna, savanna, grassland, shrubland
Pouliot et al., 2017 [34]	T	USA	2014	EF (literatures [23]), BA and fire detection (MODIS, GOES [i], and AVHRR [j] sensors)	Corn, wheat, soybean, cotton, fallow, rice, sugarcane, lentils, others
van der Werf et al., 2017 [35]	T [36,37]	World	1997–2016	EF (literatures [20,26]), BA with active fire data (MODIS, ATSR [k], and VIRS [l] sensors)	Savanna, Boreal Forest, temperate forest, tropical forest, peat, agriculture
Wu et al., 2018 [38]	T	Eastern China	2003–2015	EF (literatures [26,39]), DM (literatures), BA (MODIS sensor)	Corn, rice, wheat, cotton, rapeseed, soybean, sugarcane, peanut, potato, tobacco, sesame, sugar beet, coniferous forest, broadleaf forest, mixed forest, grassland, shrubland
Yin et al., 2019 [40]	T	China	2003–2017	EF (literatures [20]), conversion factor [27], BA with FRP data (MODIS sensor)	Forest, grassland, cropland, shrubland
Li et al., 2019 [41]	T	USA	2011, 2013–2015	EF (literature [20,26,35]), conversion factor [27], BA with FRP data (GEOS and MODIS sensors)	Forest, Savanna, Shrubs, Grasslands, Croplands
Shi et al., 2020 [42]	T	America, Africa, and Asia	2001–2017	EF [20], conversion factor [27], BA with FRP (MODIS sensor)	Forest, woody savanna, shrubland, grassland, crop, peat
Liu et al., 2019 [43]	B, hybrid-T	NW India (Punjab, Haryana)	2003–2016	EF [26], DM (field survey), DM (from GFEDv4 inventory) [35], BA (MODIS sensor with Google Earth Engine)	Rice, wheat
Liu et al., 2020 [44]	B, T	India (Punjab, Bihar, Uttar Pradesh, Haryana)	2003–2018	EF [45,46], DM (Indian statistic data and literatures [19,47–49]), BA with FRP data (MODIS and VIRS sensors)	Rice, wheat

[a] B (bottom-up); [b] EF (emission factor); [c] DM (dry mass of burned crop residue); [d] T (top-down); [e] BA (Burned area); [f] MODIS (Moderate Resolution Imaging Spectroradiometer); [g] FRP (fire radiative power); [h] SEVIRI (Spinning Enhanced Visible and Infrared Imager); [i] GOES (Geostationary Operational Environmental Satellite); [j] AVHRR (Advanced Very High-Resolution Radiometer); [k] ATSR (Along Track Scanning Radiometers); [l] VIRS (Visible and Infrared Scanner).

As shown in Figure 1, no hot spots were observed in South Korea, unlike many points in the biomass burning emissions of CO and BC over China. Thus, we believe that the top-down CRB emissions were poorly characterized in South Korea. This absence is closely related to the lower detection of the MODIS sensor for the small and short-interval fires due to its moderate spatial resolution and sparse observation frequency [44,58]. To improve the capability of the detections for small fires, many investigators have used multiple/geostationary satellite retrievals [37,51,59,60] or the hybrid MODIS-Landsat method with Google Earth Engine [43] in Table 1. Despite many efforts to improve the capability, the estimation algorithm based on satellite observations (i.e., top-down approach based on multi-sensors) is still hampered by cloud or hazy conditions [61]. Therefore, both estimations through field survey and remote sensing satellite observations compensate for mutual BB emissions [43,44].

Despite many uncertain issues in the bottom-up emission inventory, the objective is to build the bottom-up emission database of crop residue burning over South Korea. For the estimation, a field survey and combustion experiment were carried out for the 19 types of crops considered in South Korea. Thus, these activity data and emission factors are originated from actual situations in South Korea. The second objective of the study is to examine the impact of CRB emissions on the concentrations of particulate matter in South Korea.

2. Experiments and Methods

The impact of agricultural residue burning on the concentrations of particulate matter in South Korea was investigated using two different WRF-CMAQ simulations with and without the emissions of crop residue burning (CRB), denoted as "SM1" (or default) and "SM2" simulations in Figure 2, respectively. The conceptual framework of the study is given in Figure 2. For the SM2 simulation, the CRB emissions were calculated by the activity data and emission factor and analyzed spatially and temporally in detail in Section 2.2.
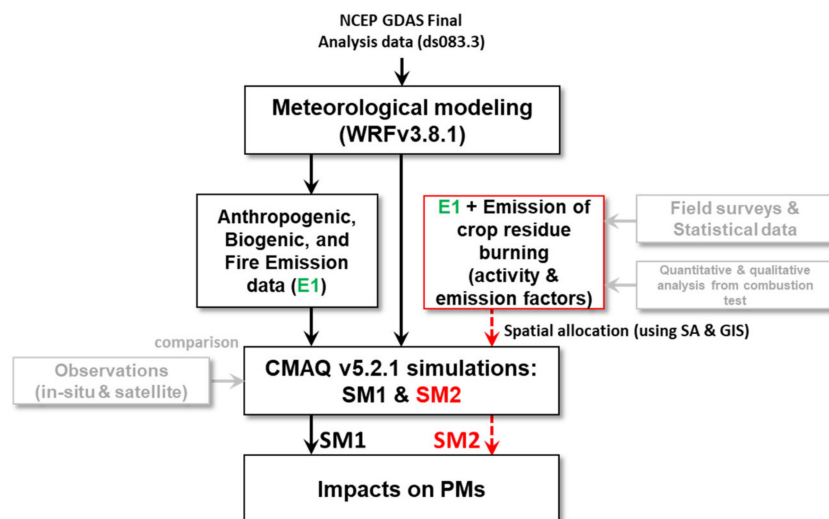
Figure 2. Process flow diagram for the study.

2.1. WRF-CMAQ Model Simulations

A 3-dimensional Eulerian Chemistry Transport Model (3D-CTM), US-EPA Models-3/CMAQ is one of the most powerful tools to manage the air quality for environmental policymakers and understand atmospheric phenomena for atmospheric scientists. The CMAQ model has been used worldwide to simulate the atmospheric levels of multi-pollutants, particularly focusing ozone and particulate matter, on local and regional scales because it is well built up and parameterized in gas-phase/heterogeneous chemistry and aerosol dynamics/thermodynamics (refer to CMAQ user's guide for more details [62,63]). In this study, we also utilized the CMAQ v5.2.1 model to simulate the air quality and examine the

impact of crop residue burning (CRB) on the levels of particulate matter in South Korea during the year of 2016 [63]. The spatial domain of the simulations consists of 273 rows and 204 columns of 15×15 km^2 resolution with 27 vertical layers from the surface to ~50 hPa over East Asia. The CMAQ model simulations were configured with Stateside Air Pollution Research Center-07 (SAPRC-07) for the gas-phase chemistry [64,65] and sixth-generation model CMAQ aerosol model (AERO6) for the aerosol dynamics [66,67]. For the horizontal advection in the CMAQ simulations, we utilized Yamartino (YAMO) scheme [68], showing good performance in terms of mass conservation [69,70]. Additionally, the Multiscale and ACM2 schemes were used for the horizontal and vertical mixing processes [71–73].

The CMAQ model was derived by the meteorological fields produced from the WRFv3.8.1 with the ARW dynamic solver [74]. The initial and boundary data were the National Center for Environmental Prediction (NCEP) Final operation global analysis (ds083.3) obtained from the NCAR (https://rda.ucar.edu accessed on 14 February 2022). These input data have a spatial resolution of $0.25° \times 0.25°$ with a 6 h interval. The WRF simulations employed the single-moment 6-class for microphysics scheme [75]. Other physical methods were Yonsei University (YSU) PBL parameterization [76], Rapid Radiative Transfer Model (RRTM) scheme for long- and short-wave radiations [77], and Kain-Fritch scheme for cumulus physics [78]. The chemical and physical parameterizations are given in Table 2.

Table 2. Configuration of the WRF/CMAQ simulations.

	Parameterizations	Schemes	Refs.
WRF	Microphysics	WSM6	[75]
	PBL	YSU	[76]
	Long and short radiations	RRTMG	[77]
	Cumulus physics	Kain-Fritsch (new Eta)	[78]
	Land surface	5-layer thermal diffusion land surface model	[79]
CMAQ	Chemical solver	EBI	[80]
	Gas phase chemistry	SAPRC-07	[64,65]
	Aerosol process	AERO6	[66,67]
	Horizontal advection	YAMO	[68]
	Vertical advection	WRF omega formula with PPM	[81,82]
	Horizontal diffusion	Multiscale	[71]
	Vertical diffusion	ACM2	[72,73]

2.2. Emission Inventory

Atmospheric levels of gaseous and particulate species are significantly influenced by emission data [83]. For anthropogenic emission, we utilized the $0.1° \times 0.1°$ resolved KORUS v5.0 emission inventory prepared from the SMOKE-Asia processing [84] over the entire domain except for South Korea. The emissions fluxes of CO, NO$_x$, SO$_2$, NH$_3$, PM$_{2.5}$, PM$_{10}$, and total VOCs from the KORUS v5.0 were replaced with those from the 1 km $\times$ 1 km resolved Clean Air Policy Support System (CAPSS) inventory for South Korea. However, the KORUS v5.0 inventory was also used for information on the VOC speciation because the CAPSS inventory provided only total VOC emission fluxes instead of the speciated VOCs. For biogenic emissions, the Model of Emissions of Gases and Aerosol from Nature—Monitoring Atmospheric Composition and Climate (MEGAN-MACC) [85] was obtained from the monthly Emission of atmospheric Compounds and Compilation of Ancillary Data (ECCAD, https://eccad.aeris-data.fr/ accessed on 14 February 2022). For the fire emission, we also took into account the daily Fire Inventory from NCAR (FINN) v1.5 (https://www.acom.ucar.eud/Data/fire/ accessed on 14 February 2022) [55]. These emission data were spatially re-gridded into the model grids for the SM1 (default) simulation. The spatial distributions of emission fluxes used in the SM1 simulation were shown over South Korea and East Asia in Figure 3 and Figure S1, respectively.
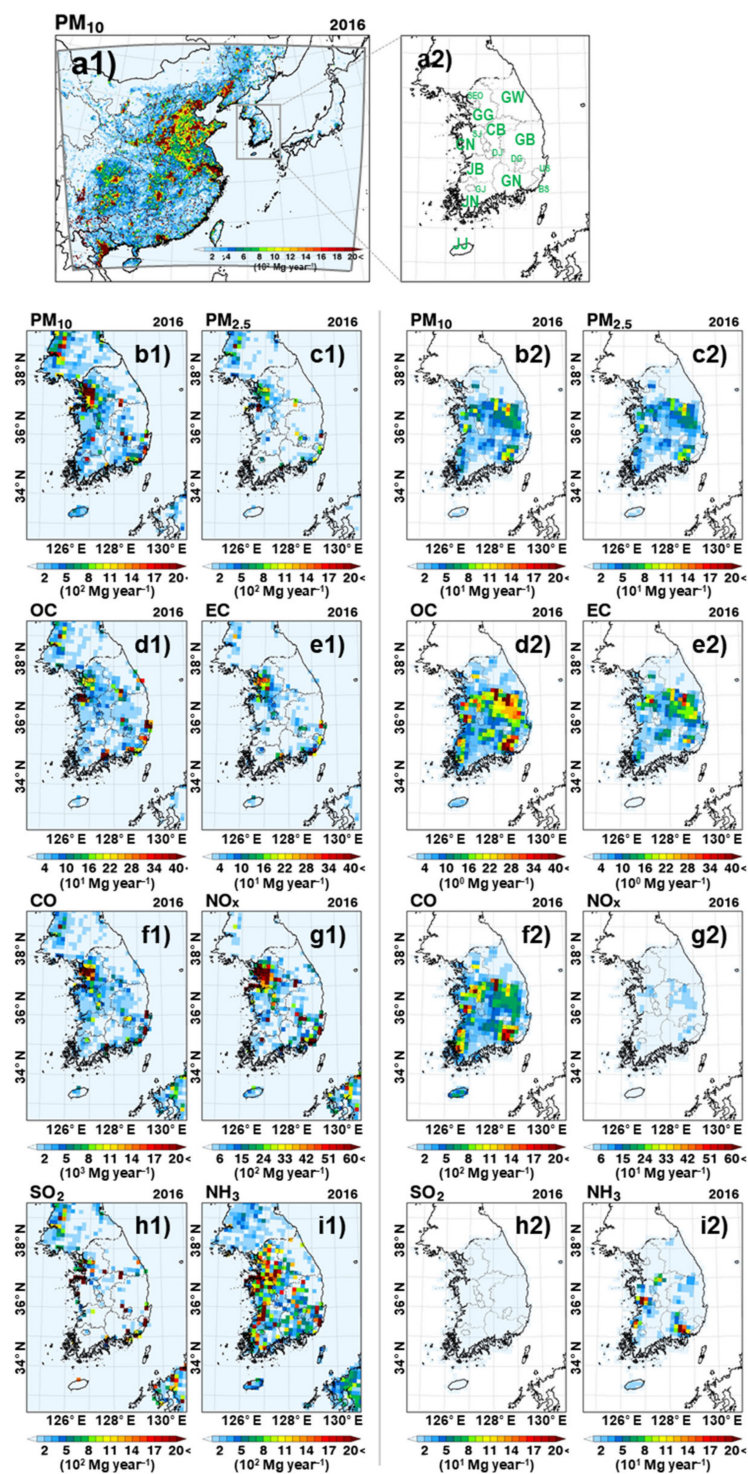
Figure 3. (**a1**) Study domain and annual emission fluxes over South Korea for (**b1**) PM_{10}, (**c1**) $PM_{2.5}$, (**d1**) OC, (**e1**) EC, (**f1**) CO, (**g1**) NO_x (as NO), (**h1**) SO_2, and (**i1**) NH_3 combined from the CAPSS, MEGAN, and FINN v1.5 inventories used in the SM1 simulations (in the left two columns). (**b2–i2**) Annual emission fluxes for the same species from the residue burning of 19 crops used in the SM2 simulation (in the right two columns). The units are small by a factor of 0.1 than those of the same species on the left columns. (**a2**) Administrative district of Seoul (SEO), BS (Busan), DG (Daegu), IC (Incheon), GJ (Gwangju), DJ (Daejeon), US (Ulsan), SJ (Sejong), GG (Gyeounggi), GW (Gangwon), CB (Chungbuk), CN (Chungnam), JB (Jeonbuk), JN (Jeonnam), GB (Gyeongbuk), GN (Gyeongnam), and JJ (Jeju).

In this study, monthly emissions of CO, NO_x, SO_2, NH_3, $PM_{2.5}$, PM_{10}, and speciated VOCs from open burning of crop residue were estimated over South Korea using several activity data and emission factors. The monthly emissions (E_{ij}) of pollutants (i) from residue burning of nineteen crops (j) were quantified from Equation (1) based on the methodology suggested by the studies of Delmas et al. [86], California Air Resources Board, US [87], and NSW Environment Protection Authority, Australia [88]. For the estimation, we considered nineteen crops, including rice (in the rice fields and ridges), barley, sweet potato, corn, soybean, pepper, sesame, perilla, peanut, garlic, onion, watermelon, apple, persimmon, citrus, pear, grape, and peach.

$$E_{i,j} = \sum_j M_j \times EF_{i,j} = \sum_j (P_j \times R_j \times D_j \times F_j) \times EF_{i,j} \tag{1}$$

where, M_j represents masses of the residue of crop type j burned in the open field (unit: kg month^{-1}) and is defined as the multiplication of P_j (production of crops, kg month^{-1}), R_j (conversion factor for crop residue production or residue-to-crop ratio), D_j (correction factor for dry matter from the crop residues), and F_j (fraction of crop residue burning in the field). The production of crops (P_j) was obtained from Statistics Korea [89]. The conversion factors (R_j) were obtained from a report of the National Institute of Agricultural Sciences (NAS) in Korea [90] and summarized in Table S1. For other activity data, we carried out surveys (e.g., face-to-face, mail, and internet surveys) on the open burning of crop residue, targeting approximately 1000 farmers. The interviewees were selected considering their distributions of the agricultural areas and farmworkers by region. The questionnaire for the survey includes (i) what fraction of each crop residue is burned in the open field, (ii) how frequently, and (iii) which season the burning occurs in. In the study, to estimate the emission factors ($EF_{i,j}$) of chemical species for 10 crops of rice, garlic, onion, sweet potato, barley, corn, peanut, watermelon, persimmon, and citrus fruit, the combustion test facility was built for the open combustion of crop residues under well-controlled conditions, which was designed based on the EPA method 5G [91]. The facility is composed of five components: (i) combustion chamber in which the crop residue is burned, (ii) inlet and outlet pipes, (iii) filter-based sampling part for PM_{10}, $PM_{2.5}$, EC, OC, and ion species, (iv) measuring part for VOCs, and (v) measuring part for other gases (e.g., NO_x, CO, SO_2, NH_3). The schematic diagram for the combustion test facility is given in Figure S2. Then, particulate matters (PM_{10} and $PM_{2.5}$) and gaseous species are analyzed qualitatively and quantitatively based on several analysis methods in Table S2. The emission factors of gaseous and particulate species were summarized in Table S3. The emission fluxes from the crop residue burning were estimated based on the municipal-level divisions (e.g., Si for the city, Gun for the county, and Gu for the district) in Korea. Finally, the emission fluxes based on the Si-Gun-Gu levels were spatially allocated to the modeling grids using the software of the Geographic Information System (GIS) and Spatial Allocator (SA). The spatial distributions of emission fluxes from the crop residue burning (CRB) were presented in the right two columns of Figure 3. The CRB emissions were then added into the default emission for the SM2 simulation.

2.3. Observations

The performance of the chemical model was evaluated by comparing the concentrations of O_3, PM_{10}, and $PM_{2.5}$ observed at ~1400 sites in China and 320 sites in South Korea. These data were collected for the entire year of 2016 from both the China National Environmental Monitoring Center (CNEMC, https://quotsoft.net/air/ accessed on 14 February 2022) [92] in China and the national air quality monitoring network (AirKorea, https://www.airkorea.or.kr/ accessed on 14 February 2022) [93] in South Korea (Figure 4).
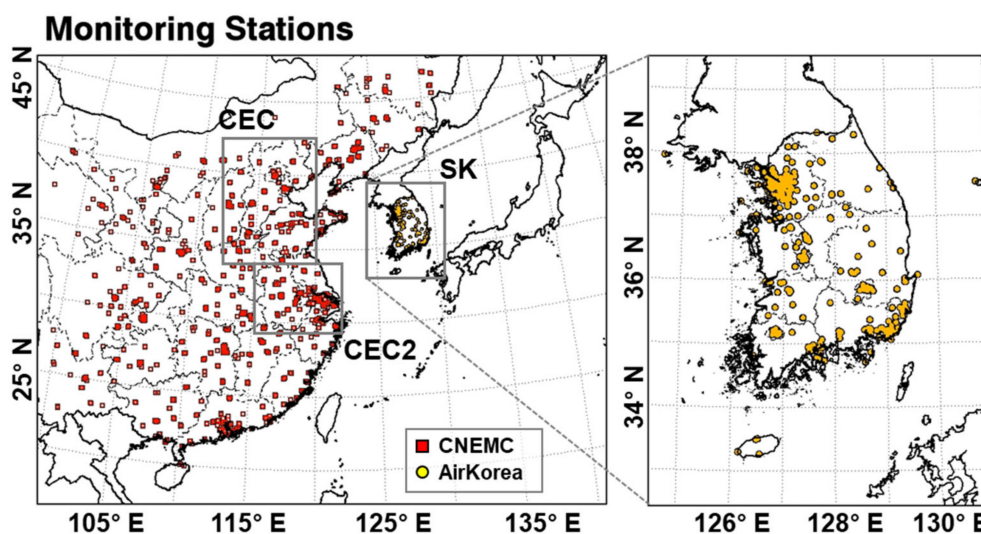
Figure 4. Analysis regions of CEC, CEC2, and SK. Monitoring stations of CNEMC (closed red squares) and AirKorea (closed yellow circles) utilized for the comparison.

In addition to the ground data, satellite-observed data were also collected from TEMIS (www.temis.nl accessed on 14 February 2022) [94] for evaluation over the entire domain. The Ozone Monitoring Instrument (OMI) observation data retrieved from the Quality Assurance for Essential Climate Variables (QA4ECV) algorithm provides the tropospheric vertical NO_2 columns on a daily basis. We extracted and utilized only valid data according to several flag criteria (e.g., processing_error_flag = 0; solar_zenith_angle < 80; snow_ice_flag < 10 or snow_ice_flag = 255; amf_trop/amf_geo > 0.2; cloud_radiance_fraction_no2 < 0.5) suggested in the document for the QA4ECV product [95]. Averaging kernels were also considered in the CMAQ-simulated NO_2 columns for direct comparison with the OMI observations [96].

3. Results and Discussion

3.1. Emission Fluxes (E) Estimated from Residue Burning of Crops over South Korea

As discussed previously in Section 2.2, the CRB emission fluxes ($E_{i,j}$) were estimated from several emission factors ($EF_{i,j}$) and activity data (M_j) related to crop residue burning. The annual emission fluxes over South Korea estimated as 9514, 8089, 4002, 2010, 172,407, 7675, 33, and 5053 Mg for PM_{10}, $PM_{2.5}$, OC, EC, CO, NO_x (as NO_2), SO_2, and NH_3, respectively (in Table 3), which corresponded to 4.16, 7.93, 8.21, 11.96, 10.27, 0.47, 0.01, and 1.86% of those from anthropogenic sources. The contributions from the crop residue burning to total emissions were not small, particularly for EC and CO, above 10%. However, such contributions can vary considerably depending on the analysis regions defined in Figure 3(a2). From a regional perspective, most species showed the highest emission fluxes in the order of Gyeongbuk (GB), Gyeongnam (GN), Chungbuk (CB), Chungnam (CN), and other provinces in Table 3. The high emissions were also clearly seen in the spatial distributions of CRB emission in Figure 3. GB province, the largest emitter of CRB, accounted for 33–41% and 14–37% for particulate and gaseous species, respectively. On the other hand, the CRB emissions in SEO, BS, DG, IC, GJ, DJ, US, and SJ were insignificant due to the limited cultivation areas in the metropolitan cities [89]. This shows a clear spatial contrast between the CRB and anthropogenic emissions (refer to Figure 3).

To evaluate the approximate magnitudes of emission fluxes in this study, we compared our estimations with data of Kim et al. (hereinafter referred to as KIM) [97], conducted for South Korea based on a similar bottom-up approach. Figure 5 showed scatter plots between KIM and our estimates for available species of $PM_{2.5}$, PM_{10}, CO, NO_x, SO_2, and NH_3. In this analysis, emission fluxes in CN province also included those of SJ province. As shown in Figure 5, many data points were significantly scattered along the 1:1 line. Those were

possibly due to two aspects. For the first, we considered seven more crops of persimmon, citrus fruit, sweet potato, rice, garlic, watermelon, and onion than those in KIM, leading to data points distributed above the 1:1 line (i.e., higher estimates). Secondly, the emission factors (EF) for barley were significantly different. The $EF_{PM2.5}$, EF_{PM10}, and EF_{CO} of KIM were 6–15 times larger than our experiment values. In contrast to the first aspect, data points can be distributed below the 1:1 line. In the scatter plot for NH_3, the large biases were determined dominantly by the high EF_{NH3} for watermelon, considered only in our estimate (Table S3). Nevertheless, both estimates were not significantly different in their magnitudes. Additionally, in both studies, GB province was ranked the highest in common for $PM_{2.5}$, PM_{10}, CO, and NO_x. Annual emission fluxes from our estimate and KIM were summarized in Table S4.

Table 3. CRB emissions of gaseous and particulate species estimated in South Korea (unit: Mg year^{-1}).

| Regions	PM_{10}	$PM_{2.5}$	OC	EC	CO	NO_x *	SO_2	NH_3
SEO	0.0	0.0	0.0	0.0	0.0	0.0	0.0	0.0
BS	0.3	0.3	0.1	0.0	4.9	0.1	0.0	0.0
DG	0.0	0.0	0.0	0.0	0.0	0.0	0.0	0.0
IC	32.7	26.0	13.7	6.2	749.0	29.4	0.2	14.4
GJ	52.0	43.5	24.8	9.3	1107.4	38.2	0.2	30.8
DJ	6.3	5.2	2.1	1.2	101.9	5.0	0.0	0.0
US	40.0	30.7	11.9	13.9	838.3	43.8	0.1	0.3
SJ	25.0	20.7	10.5	4.5	562.8	26.4	0.1	31.4
GG	521.5	411.4	208.9	124.6	10,605.2	504.9	0.9	58.4
GW	337.6	285.9	140.7	62.9	6044.8	247.3	1.2	77.0
CB	1179.3	1001.3	520.5	243.5	20,293.1	945.8	2.7	550.8
CN	1078.5	918.1	437.4	196.9	20,552.0	824.9	5.7	1237.9
JB	778.5	672.1	332.5	127.1	15,183.5	564.7	4.4	729.7
JN	815.1	675.9	333.3	155.0	24,625.4	629.6	3.9	338.9
GB	3192.3	2745.6	1327.1	828.4	39,243.3	2808.8	4.8	687.4
GN	1355.9	1166.5	600.9	229.8	27,876.3	943.0	7.4	1160.7
JJ	98.3	86.4	37.0	6.3	4619.1	62.6	1.6	135.6
sum	9513.5	8089.4	4001.6	2009.5	172,407.1	7674.7	33.1	5053.2

* NO_x emissions as NO_2.
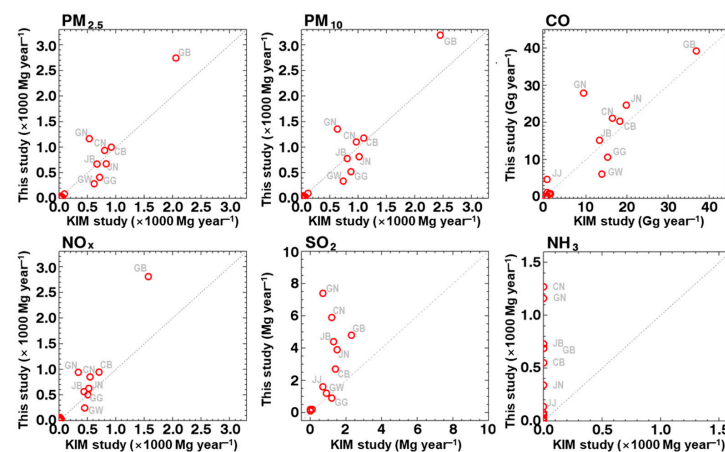
Figure 5. Scatter plots between KIM and our estimates for annual CRB emissions of 17 provinces.

Figure 6 shows monthly variations of CRB emissions of gaseous and particulate species over South Korea. As shown in Figure 6, while the CRB emission fluxes were generally high in the warm season, particularly in June for the gaseous species of CO, SO_2, and NH_3, they were great in the cold season for the particulate species of PMs, EC, and OC. Such differences are significantly related to the harvest time for the specific crop with its different emission factors for the chemical species. Accordingly, different harvest

times and emission factors for the crops also led to significant differences in the monthly contributions. For example, the contributions were generally marginal within 0.02, 1.37, and 6.10% for the gaseous species of SO_2, NO_x, and NH_3 (in the right column of Figure 6), respectively. On the other hand, the maximum contributions reached 14.25, 14.58, and 24.78% for $PM_{2.5}$, OC, and EC (in the left columns of Figure 6), respectively. The emission fluxes of EC were relatively small compared to those of PM_{10} and $PM_{2.5}$, despite it being the highest contribution.
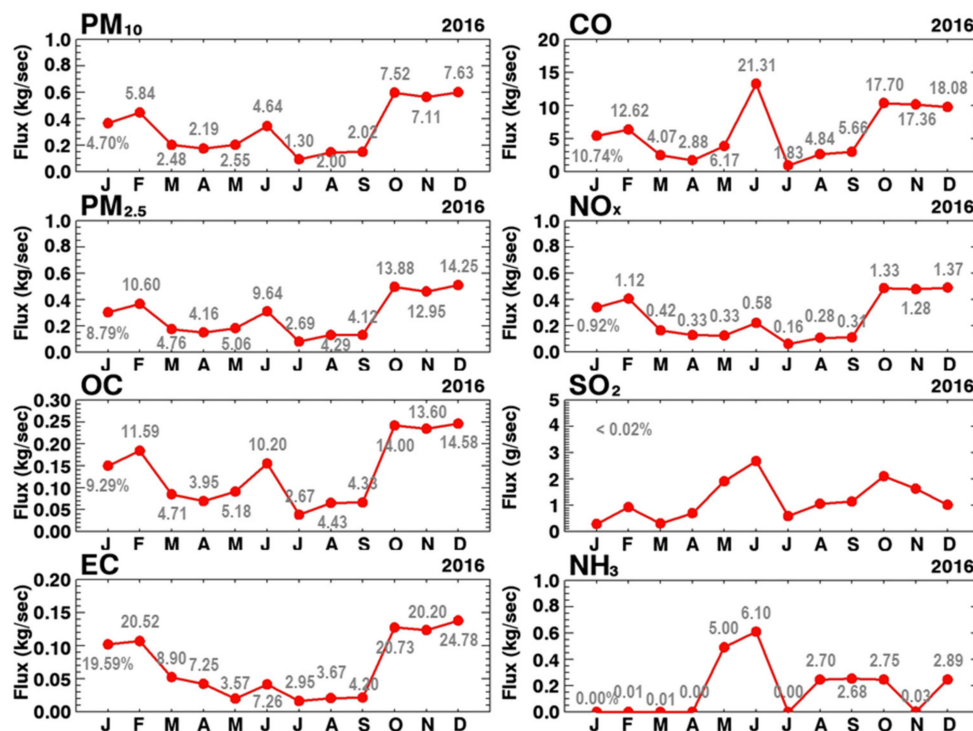
Figure 6. Monthly variations of CRB emissions for gaseous particulate species over South Korea (unit: g s^{-1} for SO_2, kg s^{-1} for other species). The numbers (unit: %) colored in gray represent contributions of CRB to total emission considering anthropogenic, biogenic, fire, and CRB sources.

For anthropogenic and CRB sources, we also examined the ratio of $PM_{2.5}$ to PM_{10} emissions in this study. The ratios can be used to identify the sources because the particulate matter in different sizes possibly originates from different sources [98,99]. In the anthropogenic emissions from the CAPSS inventory, the monthly $PM_{2.5}/PM_{10}$ ratios were almost constant, ranging between 0.41 and 0.44. For the CRB emission, the average ratio was 0.85 in the range of 0.82–0.90, indicating relatively large amounts of $PM_{2.5}$ emitted through the agricultural residue burning. Our averaging ratios for the CRB emission are similar to values from observations during the periods of biomass burning events at Gwangju Korea and Pathumthani Thailand [100,101].

3.2. Modeling Performances

We evaluated the general performances of the default CMAQ simulation (i.e., SM1) by comparing the tropospheric NO_2 columns over the entire domain. The hourly mixing ratios (unit: ppm) of NO_2 at each layer from the simulations were converted to the vertical column concentrations (unit: molecules cm^{-2}) by integrating vertically from surface to approximately 10 km in altitude for direct comparison [102].

The first and second columns of Figure 7 showed spatial and seasonal distributions of the CMAQ-calculated and OMI-retrieved NO_2 columns over East Asia. The differences and scatter plots between the two columns were presented in the third and fourth columns of Figure 7. The simulated NO_2 columns over the entire domain were 0.85×10^{15}, 0.52×10^{15},

1.12×10^{15}, 1.89×10^{15} molecules cm^{-2} for spring (March–May), summer (June–August), fall (September–November), and winter (December–February), respectively. These values were small, compared to those of OMI observation, which were 2.15×10^{15}, 1.61×10^{15}, 2.15×10^{15}, 2.87×10^{15} molecules cm^{-2} for spring, summer, fall, and winter, respectively. Despite some positive bias (showing red) partly over Hebei and Henan provinces, such negative bias (showing blue color) was seen over most regions, particularly in central east China and the Guangdong and Hong Kong areas in the third column of Figure 7 (also refer to the statistical values and slopes in the fourth column of the figure), indicating the underestimation of NO_x emissions in these areas. According to the study of ozone production efficiency (OPE) by Oak et al. [103] using KORUSv5 emission data, the OPE characteristics are best simulated when 50% of NO_x emission increase in the chemistry-transport modeling. Such results also indicate the underestimation of KORUSv5 NO_x emissions used in our study. Nevertheless, our CMAQ simulations using the same emission inventory well captured the satellite-observed spatial distributions and seasonal variations over East Asia. The correlation coefficients were quite good, ranging between 0.85 and 0.88. During the summer episode, the lower concentration observed from the OMI sensor was also well simulated by the CMAQ model in the second row of Figure 7. The low NO_2 columns in summer are attributed to the active NO_x chemical losses via the reaction of NO_2 with high concentrations of OH radicals [104,105].

In addition to satellite, in situ ground observations from the CNEMN and AirKorea were utilized to evaluate the modeling performance. The hourly observation was compared to the simulated data averaged for the pixels corresponding to the CEC, CEC2, and SK regions defined in Figure 4. Figure 8 showed the time series of hourly surface concentrations of O_3, PM_{10}, and $PM_{2.5}$ from observations (black lines) and simulations (blue lines) for CEC, CEC2, and SK in the first, second, and third columns, respectively.

In the upper panel of Figure 8, the simulated O_3 concentrations were higher by 20–25%, compared to the observation. The high O_3 mixing ratios simulated from the CMAQ simulation are strongly related to the underestimation of NO_x emissions over East Asia discussed in the NO_2 column analysis in Figure 7 because of less O_3 being titrated by NO. The correlation coefficients were good, generally ranging from 0.72 to 0.91. In Figure S3, the model-calculated O_3 mixing ratios agreed spatially with monthly averaged values of in situ observation, particularly in Seoul Metropolitan areas (showing bluish colors in the figure).

In the bottom panel of Figure 8, the simulated concentrations of PM_{10} were small by -50.8, -25.5, and -38.7%, compared to the observations over CEC, CEC2, and SK. Nevertheless, the correlation coefficients between the simulated and observed PM_{10} were moderately good (0.76 and 0.77) over CEC and CEC2. The observations captured the Asian dust in China and its impact on PM_{10} in South Korea in May and June 2016. However, the high concentrations of PM_{10} were not adequately simulated in the CMAQ simulations, in which the dust module for dust emission was off. The lower correlation coefficient in SK was mainly due to some inconsistency, particularly during April–June (refer to Figure S4). It is well known that the concentration of PM_{10} is closely related to the Asian dust event [106].

On the other hand, the temporal variations and magnitudes of observed $PM_{2.5}$ were well simulated, as shown in the middle panel of Figure 8. Accordingly, the correlation coefficients for $PM_{2.5}$ were good as 0.87, 0.84, and 0.70 over CEC, CEC2, and SK, respectively. Although the simulated $PM_{2.5}$ concentrations were also small by -27.6, -0.4, and -20.1% over the analysis regions, $PM_{2.5}$ was better simulated than PM_{10} in terms of several statistical parameters between simulations and observations (i.e., absolute and relative differences, correlation coefficient, and slope in the scatter plots). Additionally, the spatial distributions of $PM_{2.5}$ concentrations were well consistent with those of in situ observation in Figure S5. Therefore, we more focused on $PM_{2.5}$ for the impacts of crop residue burning.
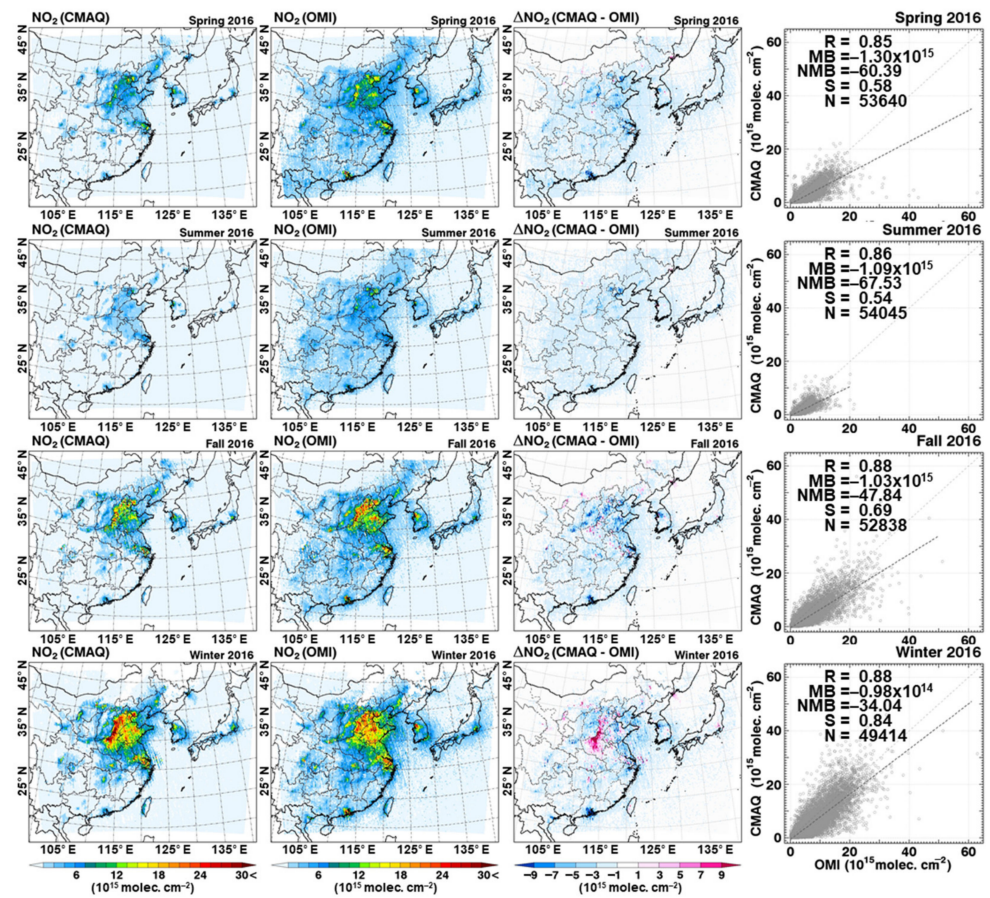
Figure 7. Spatial distributions of CMAQ-simulated and OMI-retrieved tropospheric NO$_2$ in the first and second columns. Their differences and scatter plots between two columnar NO$_2$ in third and fourth columns, respectively. In statistical analysis, R, MB, NMB, S, and N represent correlation coefficient, mean bias (molecules cm^{-2}), normalized mean bias (%), slope, and the number of data, respectively.
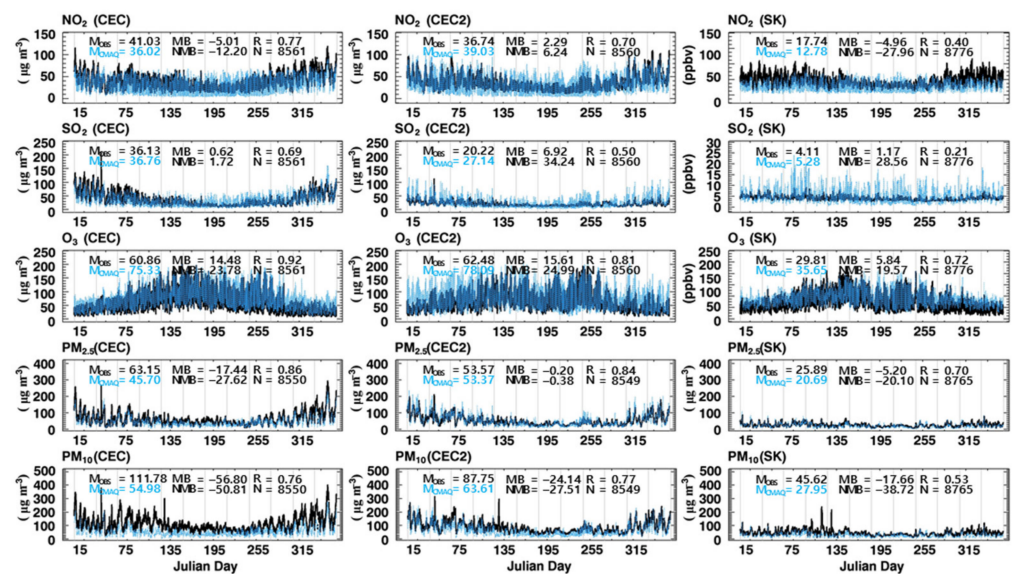
Figure 8. Time series of hourly concentrations of O$_3$, PM$_{2.5}$, and PM$_{10}$ from both observation (black lines) and simulation (blue lines) for CEC, CEC2, and SK in first, second, and third columns, respectively.

Collectively, the performance for SM1 simulation showed underestimation of PM_{10} and O_3 in the CEC region, which affects the air quality in South Korea. Nevertheless, there were relatively consistent for $PM_{2.5}$. From the statistical analysis between the simulated and observed O_3 and $PM_{2.5}$ concentrations, we believe that the SM1 simulation has sufficient performance to investigate the effect of the CRB emission on particulate matter in South Korea.

3.3. Impact of Crop Residue Burning on Particulate Matters

The impact of the crop residue burning on the concentrations of particulate matter was examined in terms of absolute (unit: $\mu g\ m^{-3}$) and relative (unit: %) differences using Equations (2) and (3) as follows:

$$A.\ Diff = C_{SM2} - C_{SM1} \tag{2}$$

$$R.\ Diff = \frac{C_{SM2} - C_{SM1}}{C_{SM1}} \times 100 \tag{3}$$

where, C_{SM1} and C_{SM2} represent the concentrations of $PM_{2.5}$ or PM_{10} from the SM1 and SM2 simulations, respectively. Figures 9 and 10 show the spatial distributions of absolute and relative differences of $PM_{2.5}$ between the SM1 and SM2 simulations over South Korea. The positive values of the absolute differences colored in red in Figure 9 indicate the elevated $PM_{2.5}$ originated from the crop residue burning. The absolute differences were lowest at $0.07\ \mu g\ m^{-3}$ in July and were generally high in June, October, November, and December (highest at $0.55\ \mu g\ m^{-3}$ in October). The monthly absolute difference increased to a maximum of $1.82\ \mu g\ m^{-3}$ at a specific pixel of GN province (defined in Figure 9) in June.
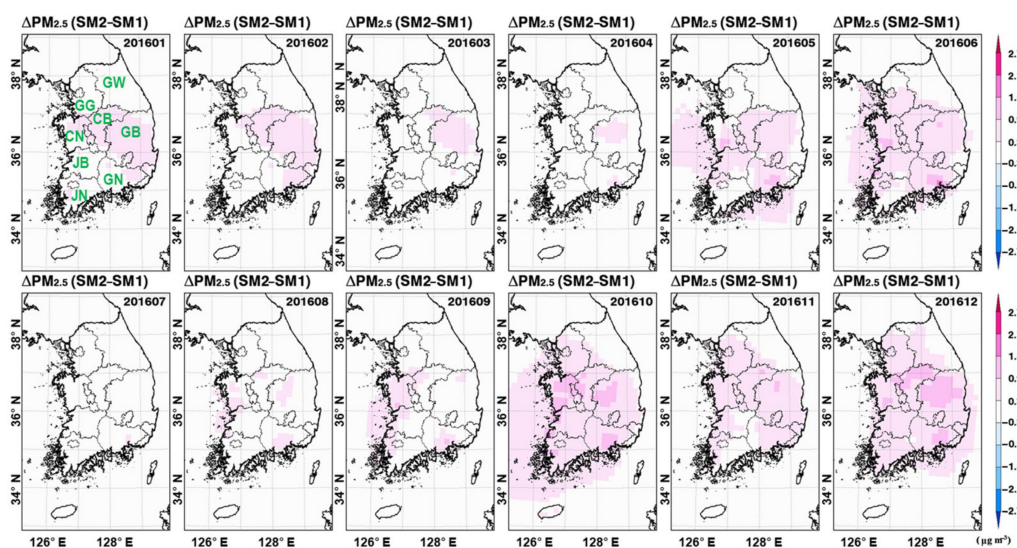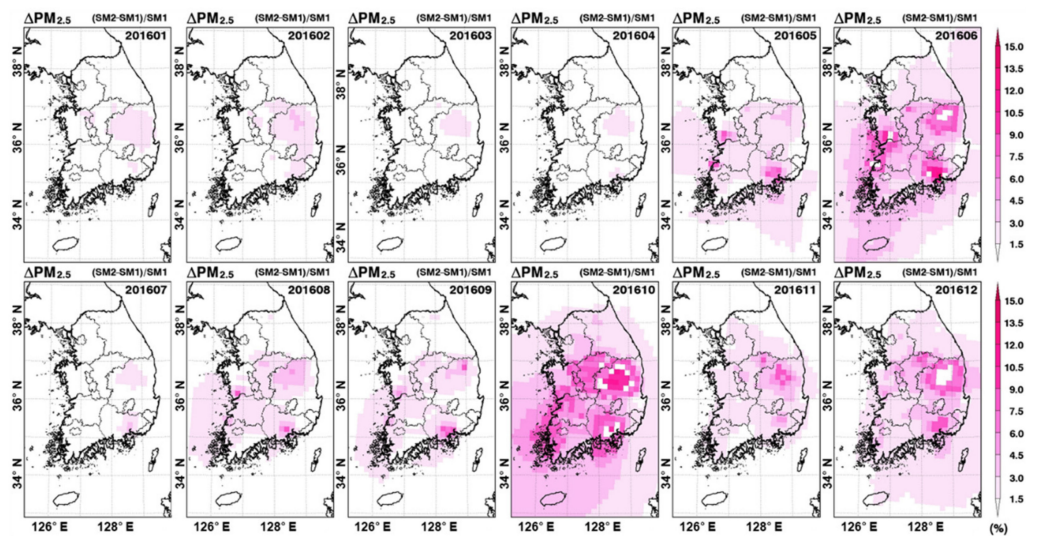

Figure 9. Spatial distributions of monthly absolute differences in $PM_{2.5}$ between SM1 and SM2 simulations (unit: $\mu g\ m^{-3}$).

The relative difference at the same specific pixel point in GN province also increased by 12.91% in June. From a temporal viewpoint, the relative differences were highest (4.33%) in October and lowest (0.60%) in March. From a spatial point of view, the relatively high elevations occurred in the rural areas of the northern GB, central GN, northern CB, southern CN areas. For PM_{10} in this study, we also examined the absolute and relative differences in Figures S6 and S7. As shown in the analysis, the temporal and spatial features for PM_{10} were not much different from those for $PM_{2.5}$.

From such analysis, most increases in the PM_{10} concentration were attributed to the increase in the $PM_{2.5}$ concentration. The result was consistent with the $PM_{2.5}/PM_{10}$ emission ratios discussed in Section 3.1. Because $PM_{2.5}$ has a more severe impact on

cardiorespiratory disorders than PM_{10}, the high ratios are more important from a public health perspective [107].

Figure 10. Spatial distributions of monthly relative differences in $PM_{2.5}$ between SM1 and SM2 simulations (unit: %).

We summarized the impacts of CRB on the monthly mean and maximum concentrations of surface $PM_{2.5}$ and PM_{10} in terms of absolute (AD) and relative differences (RD) in Tables 4 and 5. Collectively, our simulations showed that over the entire period of 2016 in South Korea, the monthly $PM_{2.5}$ (and PM_{10}) concentrations originated by the crop residue burning were elevated within 0.55 $\mu g\ m^{-3}$ (and 0.60 $\mu g\ m^{-3}$).

Table 4. Impacts of crop residue burning on the monthly concentrations of particulate matters over South Korea, in terms of absolute (AD) and relative differences (RD).

	$PM_{2.5}$		PM_{10}	
	AD ($\mu g\ m^{-3}$)	RD (%)	AD ($\mu g\ m^{-3}$)	RD (%)
January	0.21	0.81	0.23	0.76
February	0.21	0.91	0.24	0.86
March	0.17	0.60	0.18	0.55
April	0.13	0.66	0.14	0.55
May	0.29	1.79	0.31	1.33
June	0.42	3.49	0.43	2.54
July	0.07	0.68	0.07	0.49
August	0.17	1.60	0.18	1.06
September	0.21	1.59	0.22	1.14
October	0.55	4.33	0.60	3.07
November	0.34	1.97	0.38	1.67
December	0.51	2.84	0.55	2.42

The contributions from the CRB emissions to the concentrations of particulate matter estimated in this study are still subject to some uncertain issues. The uncertainty is related to the diurnal variations of the CRB emissions. Although the contributions in this study were estimated every month, the diurnal variations of CRB emissions can be randomly large. Open crop residue burning activity has often been carried out surreptitiously in the dark evening in South Korea to avoid surveillance for the illegal burning [50,108]. Thus, the peak contribution occurs possibly between late evening and early night during the day. As the planetary boundary layer (PBL) decreases at that temporal point, the surface concentrations of particulate matter or its contribution can further increase [109]. However, the time of open burning during the day varies spatially, depending on country-specific

agricultural practices [44,50]. Additionally, as input data for the estimation, the activity data still has room for improvement through the precise representativeness of the survey population to the reality.

Table 5. Impacts of crop residue burning on the maximum concentrations of particulate matter at certain pixels in South Korea, in terms of absolute (AD) and relative differences (RD).

	PM$_{2.5}$		PM$_{10}$	
	AD (µg m^{-3})	RD (%)	AD (µg m^{-3})	RD (%)
January	0.70	2.93	0.84	2.89
February	0.77	3.35	0.84	3.36
March	0.70	2.65	0.77	2.64
April	0.48	2.62	0.52	2.47
May	1.23	7.31	1.26	5.10
June	1.82	12.91	1.86	9.00
July	0.39	3.86	0.42	2.54
August	0.75	5.54	0.80	3.76
September	0.95	7.05	1.01	4.56
October	1.46	10.69	1.58	8.33
November	1.03	5.93	1.21	5.71
December	1.49	8.58	1.72	8.06

4. Summary and Conclusions

In this study, we attempted to quantify the impacts of crop residue burning (CRB) on the concentrations of PM$_{10}$ and PM$_{2.5}$ in South Korea. For the investigation, we built the CRB emission database on the basis of the bottom-up approach over South Korea. Then, two different one-year WRF-CMAQ simulations with and without the CRB emissions were conducted for 2016.

The monthly CRB emissions over South Korea were estimated using (i) several activity data of nineteen crops from the online and offline surveys with statistical data in Korea and (ii) emission factors for the gaseous and particulate species through a combustion test facility. In our estimation, the emissions of CRB over South Korea are 9514, 8089, 4002, 2010, 172,407, 7675, 33, and 5053 Mg year^{-1} for PM$_{10}$, PM$_{2.5}$, OC, EC, CO, NO$_x$ (as NO$_2$), SO$_2$, and NH$_3$, respectively. The contributions of the CRB emissions to the anthropogenic emissions were generally small, except for EC and OC, which have more than 10% contributions. In the regional comparison with the KIM study [97] over South Korea, our estimates were not significantly different except for NH$_3$ and SO$_2$ species. In both studies, Gyeongbuk (GB) province was the largest emitter of CRB emission in common for PM$_{2.5}$, PM$_{10}$, CO, and NO$_x$. The CRB emissions in GB accounted for approximately 33–41% of the total amounts for the particulate species. In terms of seasonal variation, the crop residue burning emissions were high in the cold season for PM$_{10}$, PM$_{2.5}$, EC, and OC. On the other hand, they were higher in the warm season for CO, SO$_2$, and NH$_3$.

From two different WRF-CMAQ simulations, we found the monthly average concentrations of PM$_{2.5}$ (PM$_{10}$) over South Korea were elevated between 0.07 and 0.55 µg m^{-3} (between 0.07 and 0.60 µg m^{-3}) when the CRB missions are considered in the CMAQ simulation. The elevations in PM$_{2.5}$ (PM$_{10}$) were corresponded to 0.6–4.3% (0.5–3.1%) in relative differences. The increases in PM$_{2.5}$ were high in June, October, November, and December. Spatially, the relatively high elevations occurred in the northern Gyeongbuk (GB), central Gyeongnam (GN), northern Chungbuk (CB), and southern Chungnam (CN) provinces in South Korea.

Despite large uncertainties in the activity data, our crop residue burning emission from this study is expected to be an alternative database for the areas where the satellite observations for the top-down estimation are not available, in part, for small and short-lasting fires or cloudy conditions. The emission data can also be applied to the air quality modeling to evaluate the associated disease/public health burden and impact on climate change. Finally, our analysis contributes to determining the effectiveness of the reduction

measure when the Korean government establishes the reduction policy to reduce the concentrations of PM_{10} and $PM_{2.5}$. From the study, the impact of the CRB emissions on PM_{10} and $PM_{2.5}$ were marginal over South Korea. Nevertheless, the impacts could vary significantly from a temporal and spatial point of view. Thus, further studies should investigate the in-depth diurnal/temporal variations of the crop residue burning emissions based on the combined top-down and bottom-up approaches.

Supplementary Materials: The following supporting information can be downloaded at: https://www.mdpi.com/article/10.3390/atmos13040559/s1, Figure S1: Annual emission fluxes of (a) PM_{10}, (b) $PM_{2.5}$, (c) OC, (d) EC, (e) CO, (f) NO, (g) SO_2, and (h) NH_3 combined from the KORUS v5, MEGAN, and FINN v1.5 inventories used in the SM1 simulation; Figure S2: Schematic diagram of combustion test facility; Figure S3: Spatial distributions of O_3 mixing ratios from the SM1 simulations over South Korea. The colored circles represented the observed values from the AirKorea network (unit: ppb); Figure S4: Spatial distributions of PM_{10} concentrations from the SM1 simulations over South Korea. The colored circles represented the observed values from the AirKorea network (unit: $\mu g\ m^{-3}$); Figure S5: Spatial distributions of $PM_{2.5}$ concentrations from the SM1 simulations over South Korea. The colored circles represented the observed values from the AirKorea network (unit: $\mu g\ m^{-3}$); Figure S6: Absolute differences for PM_{10}; Figure S7: Relative differences for PM_{10}; Table S1: Residue-to-crop ratios for crops considered in this study; Table S2: Analytic methods for gaseous and particulate species; Table S3: Examples of emission factors ($E_{i,j}$) of particulate and gaseous species for the crop residue (Unit: g/kg); Table S4: Estimated CRB emission and their comparison with Kim et al. [97] (unit: g/kg). Additional information are explained in [110,111] in the Supplementary Material file.

Author Contributions: Conceptualization, K.M.H. and B.T.L.; methodology, K.M.H., B.T.L., and M.-S.B.; validation, K.M.H., S.L., C.H.J., and H.S.K.; formal analysis, B.T.L., M.-S.B., C.H.J., and K.M.H.; data curation, S.L.; writing—review and editing, K.M.H., S.L., C.H.J., and B.T.L. All authors have read and agreed to the published version of the manuscript.

Institutional Review Board Statement: Not applicable.

Informed Consent Statement: Not applicable.

Data Availability Statement: Not applicable.

Conflicts of Interest: The authors declare no conflict of interest.

References

1. Kim, Y.P.; Lee, G.W. Trend of air quality in Seoul: Policy and Science. *Aerosol Air Qual. Res.* **2018**, *18*, 2141–2156. [CrossRef]
2. Koo, J.H.; Kim, J.; Lee, Y.G.; Park, S.S.; Lee, S.; Chong, H.; Cho, Y.; Kim, J.; Choi, K.; Lee, T. The implication of the air quality pattern in South Korea after the COVID-19 outbreak. *Sci. Rep.* **2020**, *10*, 22462. [CrossRef] [PubMed]
3. Ministry of Environment in South Korea. Available online: http://eng.me.go.kr/eng/web/index.do?menuId=464 (accessed on 21 January 2022).
4. World Health Organization. WHO Global Air Quality Guidelines: Particulate Matter (PM2.5 and PM10), Ozone, Nitrogen Dioxide, Sulfur Dioxide, and Carbon Monoxide. Available online: https://apps.who.int/iris/handle/10665/345329 (accessed on 21 January 2022).

5. Yevich, R.; Logan, J.A. An assessment of biofuel use and burning of agricultural waste in the developing world. *Glob. Biogeochem. Cycles* **2003**, *17*, 1095. [CrossRef]

6. Wulfhorst, J.D.; Van Tassell, L.; Johnson, B.; Holman, J.; Thill, D. *An Industry Amidst Conflict and Change: Practices and Perceptions of Idaho's Bluegrass Seed Producers*; University of Idaho College of Agricultural and Life Sciences: Moscow, ID, USA, 2006; pp. 1–20.

7. Lin, N.-H.; Tsay, S.-C.; Maring, H.B.; Yen, M.-C.; Sheu, G.-R.; Wang, S.-H.; Chi, K.H.; Chuang, M.-T.; Ou-Yang, C.-F.; Fu, J.-S.; et al. An overview of regional experiments on biomass burning aerosols and related pollutants in Southeast Asia: From BASE-ASIA and the Dongsha Experiment to 7-SEAS. *Atmos. Environ.* **2013**, *78*, 1–19. [CrossRef]

8. Zhou, L.; Baker, K.R.; Napelenok, S.L.; Pouliot, G.; Elleman, R.; O'Neill, S.M.; Urbanski, S.P.; Wong, D.C. Modeling crop residue burning experiments to evaluate smoke emissions and plume transport. *Sci. Total Environ.* **2018**, *627*, 523–533. [CrossRef] [PubMed]

9. Jethva, H.; Torres, O.; Field, R.D.; Lyapustin, A.; Gautam, R.; Kayetha, V. Connecting crop productivity, residue fires, and air quality over Northern India. *Sci. Rep.* **2019**, *9*, 16594. [CrossRef] [PubMed]

10. Takami, K.; Shimadera, H.; Uranishi, K.; Kondo, A. Impacts of Biomass Burning Emission Inventories and Atmospheric Reanalyses on Simulated PM_{10} over Indochina. *Atmosphere* **2020**, *11*, 160. [CrossRef]

11. Das, B.; Bhave, P.V.; Puppala, S.P.; Shakya, K.; Maharjan, B.; Byanju, R.M. A model-ready emission inventory for crop residue open burning in the context of Nepal. *Environ. Pollut.* **2020**, *266*, 115069. [CrossRef] [PubMed]

12. Crutzen, P.J.; Andreae, M.O. Biomass burning in the tropics: Impact on atmospheric chemistry and biogeochemical cycles. *Science* **1990**, *250*, 1669–1678. [CrossRef] [PubMed]

13. Reisen, F.; Meyer, C.P.; Keywood, M.D. Impact of biomass burning sources on seasonal aerosol air quality. *Atmos. Environ.* **2013**, *67*, 437–447. [CrossRef]

14. Agarwal, R.; Awasthi, A.; Mital, S.K.; Singh, N.; Gupta, P.K. Statistical model to study the effect of agriculture crop residue burning on healthy subjects. *MAPAN-J. Metrol. Soc. India* **2014**, *29*, 57–65. [CrossRef]

15. Awasthi, A.; Agarwal, R.; Mittal, S.K.; Singh, N.; Singh, K.; Gupta, P.K. Study of size and mass distribution of particulate matter due to crop residue burning with seasonal variation in rural area of Punjab, India. *J. Environ. Monit.* **2011**, *13*, 1073–1081. [CrossRef] [PubMed]

16. Chen, Y.; Xie, S. Characteristics and formation mechanism of a heavy air pollution episode caused by biomass burning in Chengdu, Southwest China. *Sci. Total Environ.* **2014**, *473–474*, 507–517. [CrossRef] [PubMed]

17. Yang, S.; He, H.; Lu, S.; Chen, D.; Zhu, J. Quantification of crop residue burning in the field and its influence on ambient air quality in Suqian, China. *Atmos. Environ.* **2008**, *42*, 1961–1969. [CrossRef]

18. Zhang, H.; Ye, X.; Cheng, T.; Chen, J.; Yang, X. A laboratory study of agricultural crop residue combustion in China: Emission factors and emission inventory. *Atmos. Environ.* **2008**, *42*, 8432–8441. [CrossRef]

19. Jain, N.; Bhatia, A.; Pathak, H. Emission of air pollutants from crop residue burning in India. *Aerosol Air Qual. Res.* **2014**, *14*, 422–430. [CrossRef]

20. Andreae, M.O.; Merlet, P. Emission of trace gases and aerosols from biomass burning. *Glob. Biogeochem. Cycles* **2001**, *15*, 955–966. [CrossRef]

21. Stockwell, C.E.; Christian, T.J.; Goetz, J.D.; Jayarathne, T.; Bhave, P.V.; Praveen, P.S.; Adhikari, S.; Maharjan, R.; DeCarlo, P.F.; Stone, E.A.; et al. Nepal Ambient Monitoring and Source Testing Experiment (NAMaSTE): Emissions of trace gases and lightabsorbing carbon from wood and dung cooking fires, garbage and crop residue burning, brick kilns, and other sources. *Atmos. Chem. Phys.* **2016**, *16*, 11043–11081. [CrossRef]

22. Jayarathne, T.; Stockwell, C.E.; Bhave, P.V.; Praveen, P.S.; Rathnayake, C.M.; Islam, M.R.; Panday, A.K.; Adhikari, S.; Maharjan, R.; Goetz, J.D.; et al. Nepal Ambient Monitoring and Source Testing Experiment (NAMaSTE): Emissions of particulate matter from wood and dung cooking fires, garbage and crop residue burning, brick kilns, and other sources. *Atmos. Chem. Phys.* **2018**, *18*, 2259–2286. [CrossRef]

23. McCarty, J.L. Remote Sensing-Based Estimates of Annual and Seasonal Emissions from Crop Residue Burning in the Contiguous United States. *J. Air Waste Manag. Assoc.* **2011**, *61*, 22–34. [CrossRef]

24. Turn, S.Q.; Jenkins, B.M.; Chow, J.C.; Pritchett, L.C.; Campbell, D.; Cahill, T.; Whalen, S.A. Elemental Characterization of Particulate Matter Emitted from Biomass Burning: Wind Tunnel Derived Source Profiles for Herbaceous and Wood Fuels. *J. Geophys. Res.* **1997**, *102*, 3683–3699. [CrossRef]

25. Liu, M.; Song, Y.; Yao, H.; Kang, Y.; Li, M.; Huang, X.; Hu, M. Estimating emissions from agricultural fires in the North China Plain based on MODIS fire radiative power. *Atmos. Environ.* **2015**, *112*, 326–334. [CrossRef]

26. Akagi, S.; Yokelson, R.J.; Wiedinmyer, C.; Alvarado, M.; Reid, J.; Karl, T.; Crounse, J.; Wennberg, P. Emission factors for open and domestic biomass burning for use in atmospheric models. *Atmos. Chem. Phys.* **2011**, *11*, 4039–4072. [CrossRef]

27. Wooster, M.J.; Roberts, G.; Perry, G.; Kaufman, Y. Retrieval of biomass combustion rates and totals from fire radiative power observations: FRP derivation and calibration relationships between biomass consumption and fire radiative energy release. *J. Geophys. Res. Atmos.* **2005**, *110*, D24311. [CrossRef]

28. Li, J.; Li, Y.; Bo, Y.; Xie, S. High-resolution historical emission inventories of crop residue burning in fields in China for the period 1990–2013. *Atmos. Environ.* **2016**, *138*, 152–161. [CrossRef]

29. Li, X.G.; Wang, S.X.; Duan, L.; Hao, J.; Li, C.; Chen, Y.S.; Yang, L. Particulate and trace gas emissions from open burning of wheat straw and corn stover in China. *Environ. Sci. Technol.* **2007**, *41*, 6052–6058. [CrossRef]

30. Zhang, Y.; Shao, M.; Lin, Y.; Luan, S.; Mao, N.; Chen, W.; Wang, M. Emission inventory of carbonaceous pollutants from biomass burning in the Pearl River Delta Region, China. *Atmos. Environ.* **2013**, *76*, 189–199. [CrossRef]

31. National Bureau of Statistics of China, 1991–2014. *China Statistical Yearbook*; China Statistics Press: Beijing, China, 2014.

32. Wang, X.Y.; Xue, S.; Xie, G.H. Value-taking for residue factor as a parameter to assess the field residue of field crops. *J. China Agric. Univ.* **2012**, *17*, 1–8. (In Chinese)

33. Andela, N.; Van, D.W.; Guido, R.; Kaiser, J.W.; Van Leeuwen, T.T.; Wooster, M.J.; Lehmann, C.E.R. Biomass burning fuel consumption dynamics in the tropics and subtropics assessed from satellite. *Biogeosciences* **2016**, *13*, 3717–3734. [CrossRef]

34. Pouliot, G.; Rao, V.; McCarty, J.L.; Soja, A. Development of the crop residue and rangeland burning in the 2014 National Emissions Inventory using information from multiple sources. *J. Air Waste Manag. Assoc.* **2017**, *67*, 613–622. [CrossRef]

35. Van der Werf, G.R.; Randerson, J.T.; Giglio, L.; van Leeuwen, T.T.; Chen, Y.; Rogers, B.M.; Mu, M.; van Marle, M.J.E.; Morton, D.C.; Collatz, G.J.; et al. Global fire emissions estimates during 1997–2016. *Earth Syst. Sci. Data* **2017**, *9*, 697–720. [CrossRef]

36. Giglio, L.; Randerson, J.T.; van der Werf, G.R. Analysis of daily, monthly, and annual burned area using the fourth generation global fire emissions database (GFED4). *J. Geophys. Res. Biogeosci.* **2013**, *118*, 317–328. [CrossRef]

37. Randerson, J.T.; Chen, Y.; van der Werf, G.R.; Rogers, B.M.; Morton, D.C. Global burned area and biomass burning emissions from small fires. *J. Geophys. Res.-Biogeo.* **2012**, *117*, G04012. [CrossRef]

38. Wu, J.; Kong, S.; Wu, F.; Cheng, Y.; Zheng, S.; Yan, Q.; Zheng, H.; Yang, G.; Zheng, M.; Liu, D. Estimating the open biomass burning emissions in central and eastern China from 2003 to 2015 based on satellite observation. *Atmos. Chem. Phys.* **2018**, *18*, 11623–11646. [CrossRef]

39. He, M.; Wang, X.R.; Han, L.; Feng, X.Q.; Mao, X. Emission Inventory of Crop Residues Field Burning and Its Temporal and Spatial Distribution in Sichuan Province. *Environ. Sci.* **2015**, *36*, 1208–1216. (In Chinese)

40. Yin, L.; Du, P.; Zhang, M.; Liu, M.; Xu, T.; Song, Y. Estimation of emissions from biomass burning in China (2003–2017) based on MODIS fire radiative energy data. *Biogeosciences* **2019**, *16*, 1629–1640. [CrossRef]

41. Li, F.; Zhang, X.; Roy, D.P.; Kondragunta, S. Estimation of biomass-burning emissions by fusing the fire radiative power retrievals from polar-orbiting and geostationary satellite across the conterminous United States. *Atmos. Environ.* **2019**, *211*, 274–287. [CrossRef]

42. Shi, Y.; Zang, S.; Matsunaga, T.; Yamaguchi, Y. A multi-year and high-resolution inventory of biomass burning emissions in tropical continents from 2001–2017 based on satellite observations. *J. Clean. Prod.* **2020**, *270*, 122511. [CrossRef]

43. Liu, T.; Marlier, M.E.; Karambelas, A.; Jain, M.; Singh, S.; Singh, M.K.; Gautam, R.; DeFries, R.S. Missing emissions from post-monsoon agricultural fires in northwestern India: Regional limitations of MODIS burned area and active fire products. *Environ. Res. Commun.* **2019**, *1*, 011007. [CrossRef]

44. Liu, T.; Mickley, L.J.; Singh, S.; Jain, M.; DeFries, R.S.; Marlier, M.E. Crop residue burning practices across north India inferred from household survey data: Bridging gaps in satellite observations. *Atmos. Environ. X* **2020**, *8*, 1000091. [CrossRef]

45. Andela, N.; Morton, D.C.; Giglio, L.; Paugam, R.; Chen, Y.; Hantson, S.; van der Werf, G.R.; Randerson, J.T. The Global Fire Atlas of individual fire size, duration, speed, and direction. *Earth Syst. Sci. Data* **2019**, *11*, 529–552. [CrossRef]

46. Lasko, K.; Vadrevu, K. Improved rice residue burning emissions estimates: Accounting for practice-specific emission factors in air pollution assessments of Vietnam. *Environ. Pollut.* **2018**, *236*, 795–806. [CrossRef] [PubMed]

47. Kaiser, J.W.; Andela, N.; Atherton, J.; de Jong, M.; Heil, A.; Paugam, R.; Remy, S.; Schultz, M.G.; van der Werf, G.R.; van Leeuwen, T.T.; et al. *Recommended Fire Emission Service Enhancements. ECMWF Technical Memoranda*; ECMWF: Reading, UK, 2014.

48. Bouwman, L.; Braatz, B.; Conneely, D.; Gaffney, K.; Gerbens, S.; Gibbs, M.; Hao, W.M.; Johnson, D.; Jun, P.; Lassey, K.; et al. Chapter 4: Agriculture. In *IPCC Good Practice Guidance and Uncertainty Management in National Greenhouse Gas Inventories*; IPCC-NGGIP: Kanagawa, Japan, 2000.

49. Ravindranath, N.H.; Somashekar, H.I.; Nagaraja, M.S.; Sudha, P.; Sangeetha, G.; Bhattacharya, S.C.; Abdul Salam, P. Assessment of sustainable non-plantation biomass resources potential for energy in India. *Biomass Bioenergy* **2005**, *29*, 178–190. [CrossRef]

50. Shen, Y.; Jiang, C.; Chan, K.L.; Hu, C.; Yao, L. Estimation of Field-Level NO_x Emissions from Crop Residue Burning Using Remote Sensing Data: A Case Study in Hubei, China. *Remote Sens.* **2021**, *13*, 404. [CrossRef]

51. Qiu, X.; Duan, L.; Chai, F.; Wang, S.; Yu, Q.; Wang, S. Deriving High-Resolution Emission Inventory of Open Biomass Burning in China based on Satellite Observations. *Environ. Sci. Technol.* **2016**, *50*, 11779–11786. [CrossRef] [PubMed]

52. Ellicott, E.; Vermote, E.; Giglio, L.; Roberts, G. Estimating biomass consumed from fire using MODIS FRE. *Geophys. Res. Lett.* **2009**, *36*, L13401. [CrossRef]

53. Seiler, W.; Crutzen, P. Estimates of the gross and net flux of carbon between the biosphere and the atmosphere from biomass burning. *Clim. Chang.* **1980**, *2*, 207–247. [CrossRef]

54. Kaufman, Y.J.; Justice, C.O.; Flynn, L.P.; Kendall, J.D.; Prins, E.M.; Giglio, L.; Ward, D.E.; Menzel, W.P.; Setzer, A.W. Potential global fire monitoring from EOS-MODIS. *J. Geophys. Res.* **1998**, *103*, 32215–32238. [CrossRef]

55. Wiedinmyer, C.; Akagi, S.K.; Yokelson, R.J.; Emmons, L.K.; Al-Saadi, J.A.; Orlando, J.J.; Soja, A.J. The Fire INventory from NCAR (FINN): A high resolution global model to estimate the emissions from open burning. *Geosci. Model Dev.* **2011**, *4*, 625–641. [CrossRef]

56. Wiedinmyer, C.; Yokelson, R.; Gullett, B.K. Global Emissions of Trace Gases, Particulate Matter, and Hazardous Air Pollutants from Open Burning of Domestic Waste. *Environ. Sci. Technol.* **2014**, *48*, 9523–9530. [CrossRef]

57. Van der Werf, G.R.; Randerson, J.T.; Giglio, L.; Collatz, G.J.; Mu, M.; Kasibhatla, P.S.; Morton, D.C.; DeFries, R.S.; Jin, Y.; van Leeuwen, T.T. Global fire emissions and the contribution of deforestation, savanna, forest, agricultural, and peat fires (1997–2009). *Atmos. Chem. Phys.* **2010**, *10*, 11707–11735. [CrossRef]

58. Kaiser, J.W.; Heil, A.; Andreae, M.O.; Benedetti, A.; Chubarova, N.; Jones, L.; Morcrette, J.J.; Razinger, M.; Schultz, M.G.; Suttie, M.; et al. Biomass burning emissions estimated with a global fire assimilation system based on observed fire radiative power. *Biogeosciences* **2012**, *9*, 527–554. [CrossRef]

59. Xu, W.; Wooster, M.J.; Kaneko, T.; He, J.; Zhang, T.; Fisher, D. Major advances in geostationary fire radiative power (FRP) retrieval over Asia and Australia stemming from use of Himarawi-8 AHI. *Remote Sens. Environ.* **2017**, *193*, 138–149. [CrossRef]

60. Xu, Y.; Huang, Z.; Ou, J.; Jia, G.; Wu, L.; Liu, H.; Lu, M.; Fan, M.; Wie, J.; Chen, L.; et al. Near-real-time estimation of hourly open biomass burning emissions in China using multiple satellite retrievals. *Sci. Total Environ.* **2022**, *817*, 152777. [CrossRef] [PubMed]

61. Cusworth, D.H.; Mickley, L.J.; Sulprizio, M.P.; Liu, T.; Marlier, M.E.; DeFries, R.S.; Guttikunda, S.K.; Gupta, P. Quantifying the influence of agricultural fires in northwest India on urban air pollution in Delhi, India. *Environ. Res. Lett.* **2018**, *13*, 44018. [CrossRef]

62. CMAQ User's Guide. Available online: https://github.com/USEPA/CMAQ/blob/main/DOCS/Users_Guide/README.md (accessed on 14 February 2022).

63. Byun, D.W.; Schere, K.L. Review of the governing equations, computational algorithms, and other components of the models-3 community multiscale air quality (CMAQ) modeling system. *Appl. Mech. Rev.* **2006**, *59*, 51–77. [CrossRef]

64. Hutzell, W.T.; Luecken, D.J.; Appel, K.W.; Carter, W.P.L. Interpreting predictions from the SAPRC07 mechanism based on regional and continental simulations. *Atmos. Environ.* **2012**, *46*, 417–429. [CrossRef]

65. Carter, W.P.L. Development of a condensed SAPRC-07 chemical mechanism. *Atmos. Environ.* **2010**, *44*, 5336–5345. [CrossRef]

66. Binkowski, F.; Roselle, S.J. Models-3 Community Multiscale Air Quality (CMAQ) model aerosol component 1. Model description. *J. Geophys. Res.* **2003**, *108*, 4183. [CrossRef]

67. Appel, K.W.; Pouliot, G.A.; Simon, H.; Sarwar, G.; Pye, H.O.T.; Napelenok, S.L.; Akhtar, F.; Roselle, S.J. Evaluation of dust and trace metal estimates from the Community Multiscale Air Quality (CMAQ) model version 5.0. *Geosci. Model Dev.* **2013**, *6*, 883–899. [CrossRef]

68. Yamartino, R.J. Nonnegative, Conserved Scalar Transport Using Grid-Cell-centered, Spectrally Constrained Blackman Cubics for Applications on a Variable-Thickness Mesh. *Mon. Weather Rev.* **1993**, *121*, 753–763. [CrossRef]

69. Li, X.; Rappenlück, B. A WRF-CMAQ study on spring time vertical ozone structure in Southeast Texas. *Atmos. Environ.* **2014**, *97*, 363–385. [CrossRef]

70. Rappenglück, B.; Lefer, B.; Wang, W.Y.; Czader, B.; Li, X.; Golovko, J.; Alvarez, S.; Flynn, J.; Haman, C.; Crossberg, N. *University of Houston Moody Tower 2010 Ozone Formation Research Monitoring*; Project grant No. 582-5-64594-FY10-14; Report to the Texas Commission on Environmental Quality: Houston, TX, USA, 2011; p. 98.

71. Louis, J.F. A parametric model of vertical eddy fluxes in the atmosphere. *Bound. -Layer Meteorol.* **1979**, *17*, 187–202. [CrossRef]

72. Pleim, J.E. A combined local and nonlocal closure model for the atmospheric boundary layer. Part I: Model description and testing. *J. Appl. Meteorol. Climatol.* **2007**, *46*, 1383–1395. [CrossRef]

73. Pleim, J.E. A combined local and nonlocal closure model for the atmospheric boundary layer. Part II: Application and evaluation in a mesoscale meteorological model. *J. Appl. Meteor. Climatol.* **2007**, *46*, 1396–1409. [CrossRef]

74. Skamarock, W.C.; Klemp, J.B.; Dudhia, J.; Gill, D.O.; Barker, D.; Duda, M.G.; Huang, X.Y.; Wang, W.; Powers, J.G. *A Description of the Advanced Research WRF Version 3 (No. NCAR/TN-475+STR)*; University Corporation for Atmospheric Research: Boulder, CO, USA, 2008; pp. 1–113.

75. Hong, S.-Y.; Lim, J.-O.J. The WRF Single-Moment 6-class Microphysics Scheme (WSM6). *Asia Pac. J. Atmos. Sci.* **2006**, *42*, 129–151.

76. Hong, S.Y.; Noh, Y.; Dudhia, J. A new vertical diffusion package with an explicit treatment of entrainment processes. *Mon. Weather Rev.* **2006**, *134*, 2318–2341. [CrossRef]

77. Iacono, M.J.; Delamere, J.S.; Mlawer, E.J.; Shephard, M.W.; Clough, S.A.; Collins, W.D. Radiative forcing by long-lived greenhouse gases: Calculations with the AER radiative transfer models. *J. Geophys. Res.* **2008**, *113*, D13103. [CrossRef]

78. Kain, J.S. The Kain-Fritsch convective parameterization: An update. *J. Appl. Meteor.* **2004**, *43*, 170–181. [CrossRef]

79. Dudhia, J. A multi-layer soil temperature model for MM5. In Proceedings of the 6th PSU/NCAR Mesoscale Model Users' Workshop, Boulder, CO, USA, 22–24 July 1996; pp. 49–50.

80. Hertel, O.; Berkowicz, R.; Christensen, J.; Hov, O. Test of two numerical scheme for use in atmospheric transport-chemistry models. *Atmos. Environ.* **1993**, *27A*, 2591–2611. [CrossRef]

81. CMASWIKI. *CMAQ Version 5.0 (February 2010 Release) OGD*; CMASWIKI: Research Triangle Park, NC, USA, 2015; Available online: https://www.airqualitymodeling.org/index.php/CMAQ_version_5.0_(February_2010_release)_OGD (accessed on 14 February 2022).

82. Colella, P.; Woodward, P.R. The piecewise parabolic method (PPM) for gas-dynamical simulations. *J. Comput. Phys.* **1984**, *54*, 174–201. [CrossRef]

83. Hanna, S.R.; Chang, J.C.; Fernau, M.E. Monte Carlo estimates of uncertainties in predictions by a photochemical grid model (UAM-IV) due to uncertainties in input variables. *Atmos. Environ.* **1998**, *32*, 3619–3628. [CrossRef]

84. Woo, J.H.; Choi, K.C.; Kim, H.K.; Baek, B.H.; Jang, M.; Eum, J.H.; Song, C.H.; Ma, Y.I.; Sunwoo, Y.; Chang, L.S.; et al. Development of an anthropogenic emissions processing system for Asia using SMOKE. *Atmos. Environ.* **2012**, *58*, 5–13. [CrossRef]

85. Sindelarova, K.; Granier, C.; Bouarar, I.; Guenther, A.; Tilmes, S.; Stavrakou, T.; Müller, J.-F.; Kuhn, U.; Stefani, P.; Knorr, W. Global data set of biogenic VOC emissions calculated by the MEGAN model over the last 30 years. *Atmos. Chem. Phys.* **2014**, *14*, 9317–9341. [CrossRef]

86. Delmas, R.; Lacaux, J.P.; Menaut, J.C.; Abbadie, L.; Le Roux, X.; Helaa, G.; Lobert, J. Nitrogen compound emission from biomass burning in tropical African Savanna FOS/DECAFE 1991 experiment. *J. Atmos. Chem.* **1995**, *22*, 175–193. [CrossRef]

87. CARB. *Area-Wide Source Methodology, Section 7.17 Agricultural Burning and Other Burning Methodology*; California Air Resource Board: Sacrameto, CA, USA, 2005.

88. NSW EPA. *Air Emissions Inventory for the Greater Metropolitan Regions in New South Wales, 2008 Calendar Year, Biogenic and Geogenic Emissions: Results, Technical Report No. 2*; NSW EPA: Sydney, Australia, 2012; pp. 19–35.

89. Statistics Korea. Available online: https://kosis.kr (accessed on 1 January 2022).

90. National Institute of Agricultural Sciences (NAS). *Establishment and Assessment of Biomass Inventory for Bioenergy*; NAS: Wanju, Korea, 2013; pp. 1–199.

91. Environmental Protection Agency. *Determination of Particulate Emissions form Wood Heaters from a Dilution Tunnel Sampling Location*; 40 US code of Federal Regulations, Part 60, Appendix A, Method 5G, U.S.; Government Print Office: Washington, DC, USA, 2000.

92. CNEMC. Available online: https://quotsoft.net/air/ (accessed on 1 January 2022).

93. AirKorea. Available online: https://www.airkorea.or.kr/ (accessed on 1 January 2022).

94. TEMIS. Available online: www.temis.nl (accessed on 1 January 2022).

95. Boersma, K.F.; Eskes, H.; Richter, A.; De Smedt, I.; Lorente, A.; Beirle, S.; Van Geffen, J.; Peters, E.; Van Roozendael, M.; Wagner, T. *QA4ECV NO2 Tropospheric and Stratospheric Vertical Column Data from OMI (Version 1.1) [Data Set]*; Royal Netherlands Meteorological Institute (KNMI): De Bilt, The Netherland, 2017. [CrossRef]

96. Eskes, H.J.; Boersma, K.F. Averaging kernels for DOAS total-column satellite retrievals. *Atmos. Chem. Phys.* **2003**, *3*, 1285–1291. [CrossRef]

97. Kim, D.Y.; Choi, M.A.; Han, Y.H.; Park, S.K. A study on estimation of air pollutants emission from agricultural waste burning. *J. Korean Soc. Atmos. Environ.* **2016**, *32*, 167–175. [CrossRef]

98. Chan, C.K.; Yao, X. Air pollution in mega cities in China. *Atmos. Environ.* **2008**, *42*, 1–42. [CrossRef]

99. Zhao, D.; Chen, H.; Yu, E.; Luo, T. $PM_{2.5}/PM_{10}$ ratios in eight economic regions and their relationship with meteorology in China. *Adv. Meteorol.* **2019**, *2019*, 5295726. [CrossRef]

100. Ryu, S.Y.; Kwon, B.G.; Kim, Y.G.; Kim, H.H.; Chun, K.J. Characteristics of biomass burning aerosol and its impact on regional air quality in the summer of 2003 at Gwangju, Korea. *Atmos. Res.* **2007**, *84*, 362–373. [CrossRef]

101. Kim Oanh, N.T.; Ly, B.T.; Tipayarom, D.; Manandhar, B.R.; Prapat, P.; Simpson, C.D.; Liu, L.J.S. Characterization of particular matter emission from open burning of rice straw. *Atmos. Environ.* **2011**, *45*, 493–502. [CrossRef] [PubMed]

102. Herron-Thorpe, F.L.; Lamb, B.K.; Mount, G.H.; Vaughan, J.K. Evaluation of a regional air quality forecast model for tropospheric NO_2 columns using the OMI/Aura satellite tropospheric NO_2 product. *Atmos. Chem. Phys.* **2010**, *10*, 8839–8854. [CrossRef]

103. Oak, Y.J.; Park, R.J.; Schroeder, J.R.; Crawford, J.H.; Blake, D.R.; Weinheimer, A.J.; Woo, J.H.; Kim, S.W.; Yeo, H.; Fried, A.; et al. Evaluation of simulated O_3 production efficiency during the KORUS-AQ campaign: Implications for anthropogenic NO_x emissions in Korea. *Elem. Sci. Anth.* **2019**, *7*, 56. [CrossRef]

104. Han, K.M.; Song, C.H.; Ahn, H.J.; Park, R.S.; Woo, J.H.; Lee, C.K.; Richter, A.; Burrows, J.P.; Kim, J.Y.; Hong, J.H. Investigation of NO_x emissions and NO_x-related chemistry in East Asia using CMAQ-predicted and GOME-derived NO_2 columns. *Atmos. Chem. Phys.* **2009**, *9*, 1017–1036. [CrossRef]

105. Han, K.M.; Lee, S.; Chang, L.S.; Song, C.H. A comparison study between CMAQ-simulated and OMI-retrieved NO_2 columns over East Asia for evaluation of NO_x emission fluxes of INTEX-B, CAPSS, and REAS inventories. *Atmos. Chem. Phys.* **2015**, *15*, 1913–1938. [CrossRef]

106. Chun, Y.; Cho, H.K.; Chung, H.S.; Lee, M. Historical records of Asian dust events (Hwangsa) in Korea. *Bull. Amer. Meteor. Soc.* **2008**, *89*, 823–827. [CrossRef]

107. Pope, C.A., III; Dockery, D.W. Health effects of fine particulate air pollution: Lines that connect. *J. Air Waste Manag. Assoc.* **2006**, *56*, 709–742. [CrossRef] [PubMed]

108. Jung, J.S.; Kang, J.H. Postharvest Burning of Crop Residues in Home Stoves in a Rural Site of Daejeon, Korea: Its Impact to Atmospheric Carbonaceous Aerosol. *Atmosphere* **2021**, *12*, 257. [CrossRef]

109. Pan, L.; Xu, J.; Tie, X.; Mao, X.; Gao, W.; Chang, L. Long-term measurements of planetary boundary layer height and interactions with $PM_{2.5}$ in Shanghai, China. *Atmos. Pollut. Res.* **2019**, *10*, 989–996. [CrossRef]

110. NAS. *Establishment and Assessment of Biomass Inventory for Bioenergy*; National Institute of Agricultural Sciences: Wanju, Korea, 2013.

111. KEITI. *Improvement of Air Pollution Emission Data by Biomass Burning*; Korea Environmental Industry and Technology Institute: Seoul, Korea, 2014.